Chirality Bias Tissue Homeostasis by Manipulating Immunological Response

Shengjie Jiang, Qiang Zeng, Kai Zhao, Jinying Liu, Qiannan Sun, Kang Huang, Ying He, Xuehui Zhang, Hui Wang, Xinghua Shi, Chuanliang Feng,* Xuliang Deng,* and Yan Wei*

The physiological chirality of extracellular environments is substantially affected by pathological diseases. However, how this stereochemical variation drives host immunity remains poorly understood. Here, it is reported that pathology-mimetic M-nanofibrils—but not physiology-mimetic P-nanofibrils—act as a defense mechanism that helps to restore tissue homeostasis by manipulating immunological response. Quantitative multi-omics in vivo and in vitro shows that M-nanofibrils significantly inhibit inflammation and promote tissue regeneration by upregulating M2 macrophage polarization and downstream immune signaling compared with P-nanofibrils. Molecular analysis and theoretical simulation demonstrate that M-chirality displays higher stereoaffinity to cellular binding, which induces higher cellular contractile stress and activates mechanosensitive ion channel PIEZOl to conduct Ca^{2+} influx. In turn, the nuclear transfer of STAT is biased by Ca^{2+} influx to promote M2 polarization. These findings underscore the structural mechanisms of disease, providing design basis for immunotherapy with bionic functional materials.

1. Introduction

Regulation of immunological response is the key for maintenance and recovery of host homeostasis over the course of life.[1] As one of the most critical biochemical signatures of life, the assembly of chiral molecule to supra-molecular chiral structure is crucial for the well implementation of sophisticated functions involved in life process.[2] In addition, the physiological chirality both at molecular and supra-molecular level constantly transform due to aging or pathological condition.[3] As such, much attention has been paid on the influence of different chirality on immunity.

The molecular chirality, as basic building blocks of living organisms, was established to undergo remarkable racemization due to aging.[4] The ratio of D- to L-chiral molecules in teeth or bone has been used to estimate ages in forensic medicine.[5] Free D-amino acid chirality was found to stimulate M1 macrophages and myeloid cells and promote survival of intestinal naïve B cells.[6] Free L-isomers were proven to lead better activation of macrophages, B cells, dendritic cells, and CD8+ T cells than D isomers.[7] Furthermore, chiral molecules immobilized on 2D material surfaces or introduced into 3D thermogels were reported to regulate the adhesion and activation of macrophages or neutrophils for control of inflammation.[8] These studies displayed that molecular chirality can interact with immune cells and elicit distinct cellular behaviors.

However, the chiral molecules that support cell functions do not exist in isolation but are assembled into much complex supramolecular structures.[9] Moreover, the chiral architectural environments in life body can be conversed upon the context of

S. Jiang, Q. Zeng, K. Zhao, Q. Sun, Y. He, X. Deng, Y. Wei
Beijing Laboratory of Biomedical Materials
Department of Geriatric Dentistry
Peking University School and Hospital of Stomatology
Beijing 100081, P. R. China
E-mail: kqdengxuliang@bjmu.edu.cn; kqweiyan@bjmu.edu.cn
S. Jiang, Q. Zeng, K. Zhao, Q. Sun, Y. He, X. Deng, Y. Wei
Institute of Medical Technology
Peking University Health Science Center
Beijing 100191, P. R. China
J. Liu
Key Laboratory for Special Functional Materials of Ministry of Education
School of Materials Science and Engineering
Henan University
Kaifeng 475004, P. R. China

K. Huang, H. Wang, X. Shi
CAS Key Laboratory of Nanosystem and Hierarchical Fabrication
Laboratory of Theoretical and Computational Nanoscience
CAS Key Laboratory for Biomedical Effects of Nanomaterials and Nanosafety
CAS Center for Excellence in Nanoscience
National Center for Nanoscience and Technology
Beijing 100190, P. R. China
X. Zhang
Department of Dental Materials and Dental Medical Devices Testing Center
National Engineering Laboratory for Digital and Material Technology of Stomatology
Peking University School and Hospital of Stomatology
Beijing 100081, P. R. China
C. Feng
State Key Laboratory of Metal Matrix Composites
School of Materials Science and Engineering
Shanghai Jiaotong University
Shanghai 200240, P. R. China
E-mail: clfeng@sjtu.edu.cn

**ADVANCED
SCIENCE NEWS**

www.advancedsciencenews.com

**ADVANCED
MATERIALS**

www.advmat.de

health or disease. Physiologically, right-handedness (P chirality) is the predominant structural characteristics of extracellular matrix since its main component of collagen is composed by right-handed fibrils.[10] In contrast, left-handedness (M chirality) is present in pathological conditions in which proteins with right-handed architectures arise in various organs, such as amyloid fibrils as a hallmark of Alzheimer's disease, cerebral angiopathy, and systematic amyloidosis, where the immune cells together with the released inflammatory mediators will greatly affect the disease progress.[11] Therefore, the immune cells recruited to healthy or diseased local tissue are exposed to different chiral structural cues. Although the distinct preference for chiral structures in physiological or pathological conditions is a key extracellular environmental parameter, little is known about how this natural stereochemical bias manipulates the immunological response. Experimental advances in this area may contribute to an improved understanding of the structural mechanisms of aging and disease.

In the present study, we report that pathology-mimetic M-nanofibrils attempt to restore tissue homeostasis by inhibiting inflammation and promoting regeneration more than physiology-mimetic P-nanofibrils (**Figure 1**a). The immunological response and spatiotemporal signaling cascades of macrophages upon 3D chirality were investigated by quantitative multi-omics in vivo and in vitro. The heterogeneity in the interfacial enantioselective mechanism was theoretically studied by classical molecular dynamics simulation. Understanding the chirality-dependent immunological response would offer the possibility of developing material strategies for regulating macrophages to treat disease.

2. Results and Discussion

By assembling D-molecule into M-nanofibrils and L-molecule into P-nanofibrils, biomimetic chiral matrixes were synthesized, which simultaneously mimicked both the molecular-level and supra-molecular-level chirality of extracellular microenvironments in physiological and pathological conditions.[3] Spiral nanofibrils were fabricated by the self-assembly of a low-molecular-weight hydrogelator C_2-symmetric phenylalanine derivative through hydrogen bonding and π–π stacking interaction (Figure 1b). Matrix chirality was characterized by scanning electron microscopy (SEM) and circular dichroism (CD). The physiology-mimetic P-nanofibrils and pathology-mimetic M-nanofibrils matrixes showed a perfect mirror–image relationship (Figure 1c), with an isodichroic point, zero crossing at 239 nm, and a strong (273 nm) and weak (228 nm) CD signals, and the opposite VCD patterns of the amide I stretching band at around 1636 cm^{-1} (Figure 1d,e). These matrixes presented different chiral nanostructures but almost the same chemical and physical properties, including the diameter (80 nm), helical pitch of the nanofibers (1.5 µm), and stiffness (storage modulus $G' \approx 2500$ Pa and loss modulus $G'' \approx 500$ Pa) (Figure 1f,g). Therefore, these matrixes provide a favorable platform to study the effect of chiral nanostructure on immunological response independent of other matrix properties.

To assess the effects of chirality in vivo, the rat calvarial defect model was chosen to represent the osteoimmunological

model.[12] All animal experiments were conducted with the approval of the Animal Care and Use Committee of Peking University (IACUC No. LA2021077). The pathology-mimetic M-nanofibril matrix and physiology-mimetic P-nanofibril matrix were implanted in rat cranial defects covered with non-absorbable membrane barriers. Three days after implantation, immunohistochemical staining and quantitative analysis indicated that the expression of IL-10 and COL9A2 in the defect area were significantly upregulated in the M group compared with the P group (**Figure 2**a–c). Seven days after implantation, the expression of COL9A2 in the defect area was still upregulated in the M group, whereas similar expression of IL-10 was found in the two groups (Figure 2a,b and Figure S1, Supporting Information). IL-10 is a typical anti-inflammatory factor that inhibits T cell cloning and IFNγ synthesis.[13] COL9A2 is a structural constituent of the extracellular matrix beneficial for tissue regeneration.[14] These data demonstrate that the M nanofibrils inhibited inflammation and promoted tissue regeneration to restore tissue homeostasis in comparison with the P nanofibrils at the early stage. Recently, it was demonstrated that L-amyloid β-protein and α-synuclein associated with Alzheimer's disease, Parkinson's disease, and amyotrophic lateral sclerosis act as an antimicrobial peptide, whereas islet amyloid polypeptide (IAPP) associated with type II diabetes reduces cell toxicity.[15] Together with these findings, our results suggest that the structure of these pathological proteins also plays a vital role as a protective mechanism to resist disease.

The direction of macrophage polarization plays a crucial role in ensuring rapid response to microenvironmental changes for restoring tissue homeostasis. It is well established that M2 macrophages help to inhibit inflammation and promote tissue regeneration, whereas M1 macrophages have the opposite effects.[16] Therefore, the cell composition in the defect areas was analyzed to explore the possible explanation for the chirality-dependent variation in inflammation and regeneration. At day 3, the number of macrophages with the M2 surface marker CD206 was higher in the M group than in the P group, whereas the proportion of macrophages with the M1 surface marker CCR7 in both groups was similar (Figure 2d and Figure S2, Supporting Information). At day 7, the proportion of different phenotypes of macrophages in the chiral matrix implantation area tended to be similar in both groups. We found that the macrophages with M1 and M2 markers in the PBS implanted control group were significantly weaker than that in the P-nanofibril matrix and in the M-nanofibril matrix (Figure S3, Supporting Information). This phenomenon suggested that M-nanofibrils facilitate M2-type polarization of macrophages to a greater extent than P-nanofibrils in the early stage of defect repair. Furthermore, flow cytometry and protein profile of tissue fluid of the defect area showed that the ratios of integrin β1 (Itgβ1) and PIEZO1 positive cells in the M-nanofibril matrix were significantly higher than that in the P-nanofibril matrix and in control group (Figure 2e and Figure S3, Supporting Information), paving the way for upregulated M2-type polarization of macrophages by M-nanofibrils.[17]

To investigate the downstream functional effects induced by the chirality-dependent polarization of macrophages, high-throughput sequencing of the complex proteins in the tissue fluid was also conducted. Pathway enrichment analysis showed
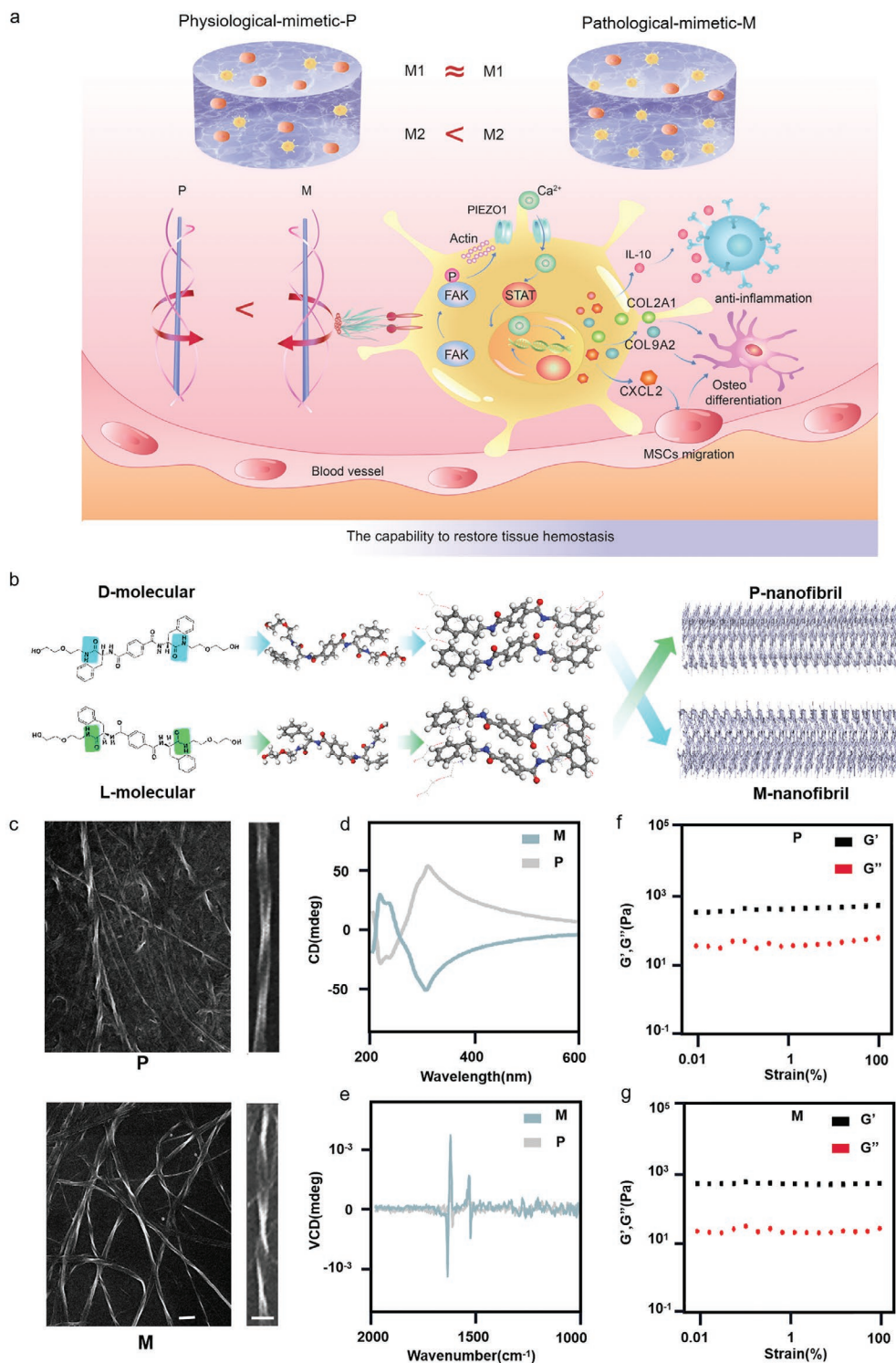
Figure 1. Pathology-mimetic M-nanofibrils act as a defense mechanism that helps to restore tissue homeostasis than physiology-mimetic P-nanofibrils. a) A schematic representation of chirality-dependent immunological response and downstream effect on tissue homeostasis. b) A schematic representation of chiral spiral nanofibrils fabrication by the self-assembly of a low-molecular-weight hydrogelator C_2-symmetric phenylalanine derivative through hydrogen bonding and π–π stacking interaction. c) Scanning electron microscopy images of right-handed (P) and left-handed (M) chiral matrixes after drying. Scale bars: 200 nm. d,e) The circular dichroism spectra of enantiomers hydrogels in PBS and vibrational circular dichroism (VCD) spectroscopy (symbols) of the enantiomers xerogel. f,g) The two matrixes presented almost the same stiffness (storage modulus $G' \approx 2500$ Pa and loss modulus $G'' \approx 500$ Pa).
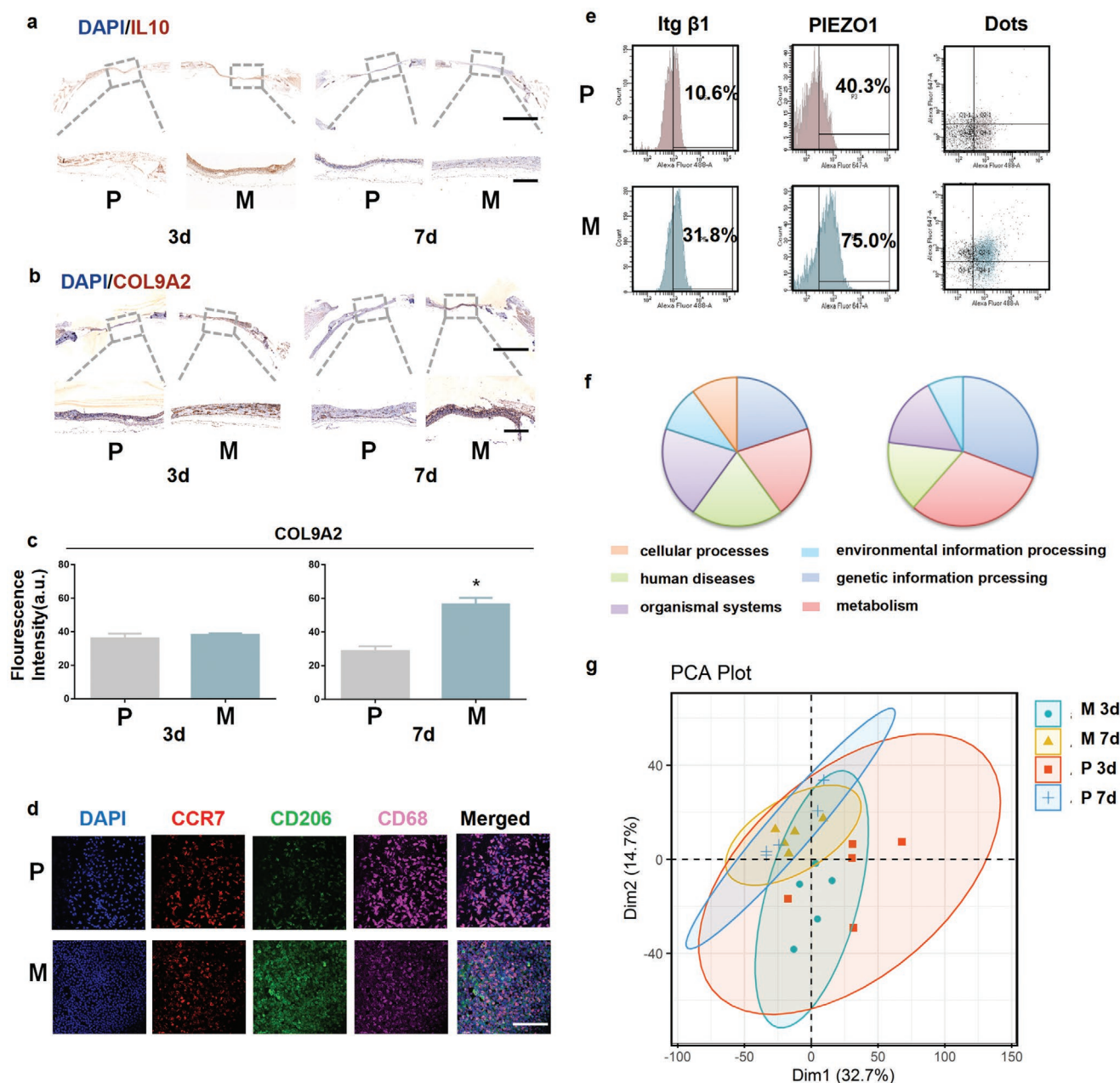
Figure 2. M-nanofibrils significantly inhibited inflammation and promoted tissue regeneration in vivo compared with P-nanofibrils. a,b) Histological analysis shows that IL-10 and COL9A2 expression in the defect area was significantly upregulated in M-nanofibrils compared with that in P-nanofibrils. c) Quantification of fluorescence intensity shows that the expression of COL9A2 was higher in the M-nanofibrils than in the P-nanofibrils at day 7. d) Immunofluorescence staining shows that the expression of the M2 surface marker CD206 was higher in the M-nanofibrils than in the P-nanofibrils at day 7. Scale bars: 100 µm. e) Flow cytometry assay showing that positive co-expression of Itgβ1 and PIEZO1 in cells was higher in the M-nanofibril matrix. High-throughput sequencing of the complex proteins in tissue fluid: f) pathway enrichment analysis showing the functions of the upregulated proteins, g) principal component analysis (PCA) showing that the macrophage phenotype in the M group was different from that in the P group at day 3 but similar at day 7. Data are the means ± SEM. *$P < 0.05$; two-tailed unpaired Student's t-test (c).

that the upregulated proteins in 3 and 7-d M group were mainly functionally enriched in cellular processes, environmental information processing, human diseases, genetic information processing, organismal systems, and metabolism (Figure 2f), indicating that the M2-type polarization of macrophages induced by M-nanofibril matrix secreted various proteins that perform early tissue repair functions. Principal component analysis

(PCA) showed that day 3 proteins in the M-nanofibril matrix were different from those in the P-nanofibril matrix, whereas day 7 proteins in the two groups was similar (Figure 2g), which was consistent with the trend in cell composition analysis and implied that significant differences arose in the phenotype and functions of macrophages recruited by different chiral microenvironments at the early stage after implantation. Taken
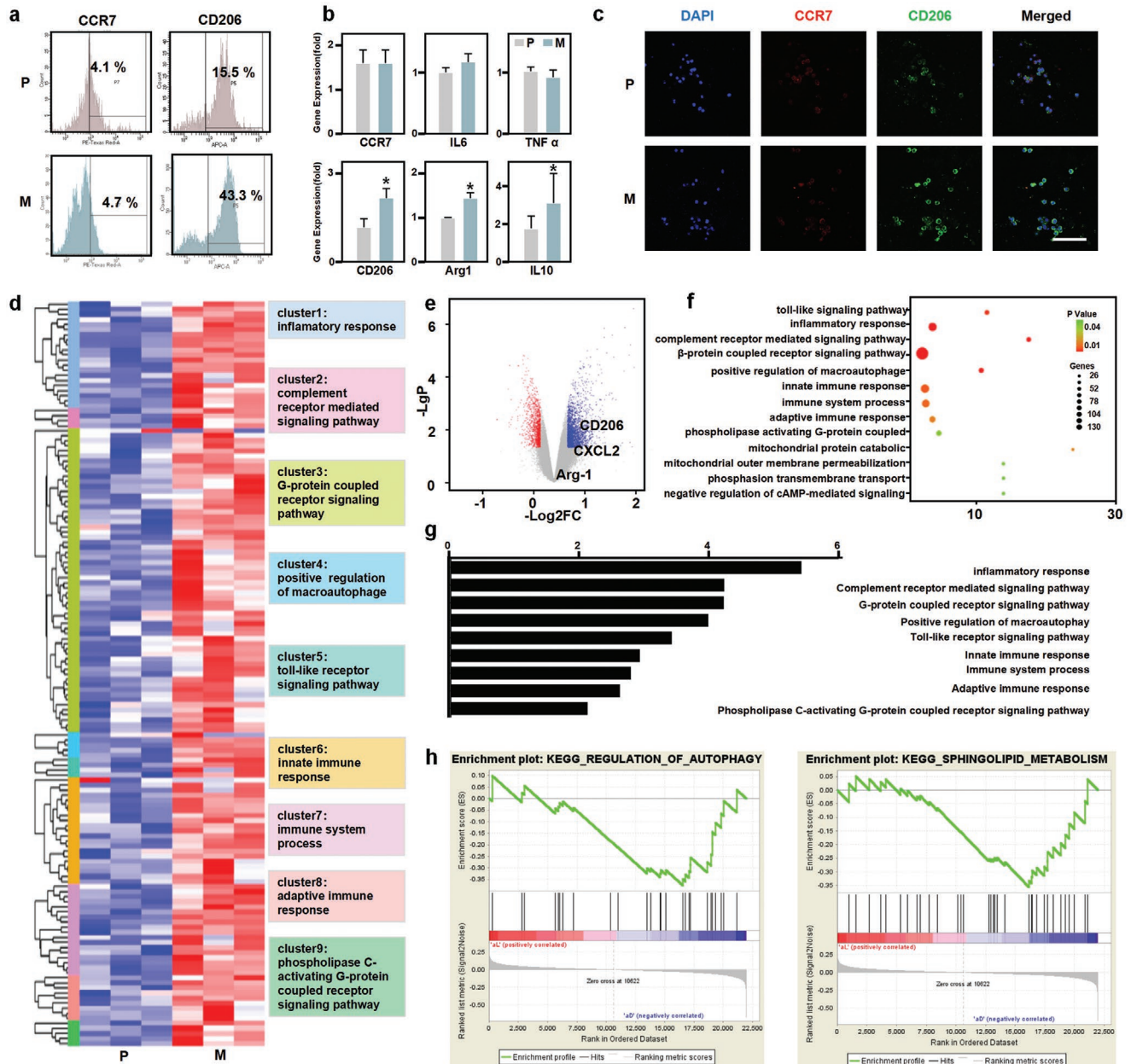
Figure 3. M-nanofibrils upregulated M2 macrophage polarization and downstream immune signaling in vitro compared with P-nanofibrils. a) Flow cytometry shows that the expression of CD206 was significantly upregulated in the M-nanofibrils compared with that in the P-nanofibril matrix, whereas similar expression levels of CCR7 were found in both groups. b) RT-qPCR shows that the gene expression of M2 marker *ARG1* and anti-inflammatory factor *IL10* was upregulated in the M group, whereas the expression of M1-related pro-inflammatory factors *TNFα* and *IL6* showed no significant difference between the two groups. c) Immunofluorescence staining shows that the expression of CD206 was significantly higher in the M-nanofibril matrix than in the P-nanofibril matrix. d) Hierarchical gene clustering shows that the overexpressed genes of macrophages in the M group were mainly related to the biological process of immune response. e) Volcano plot, f) enriched gene ontology terms, and g) pathway enrichment analysis show that the expression of *CD206* and *ARG1* and M2-related pathways was upregulated in the M group compared with the P group. h) Gene enrichment analysis revealed that autophagy- and sphingolipid metabolism-related genes associated with M2 polarization were enriched in the M group. Data are the means ± SEM. *$P < 0.05$; two-tailed unpaired Student's t-test (b).

together, our data demonstrate that M-nanofibrils possessed higher capability for restoration of tissue homeostasis through upregulation of M2 macrophage polarization than P-nanofibrils.

After establishing the functional role of chirality in immune response in vivo, we further explored the effect of chirality in vitro. A cell counting kit-8 (CCK-8) assay (Figure S4, Supporting Information) showed that M and P matrixes had similar biocompatibility to encapsulated macrophages. Flow cytometry detected that the expression of CD206 was significantly upregulated in the M- than in the P-nanofibril matrix. Similar expression levels of CCR7 were found in both groups (**Figure 3**a). This phenomenon was supported by the immunofluorescence

**ADVANCED
SCIENCE NEWS**
www.advancedsciencenews.com

**ADVANCED
MATERIALS**
www.advmat.de

and RT-qPCR results (Figure 3b,c). The gene expression of M2 marker *ARG1* and anti-inflammatory factor *IL10* was upregulated in the M group, whereas expression of the M1-related pro-inflammatory factors *TNF-α* and *IL6* showed no significant difference between the two groups (Figure 3b). Macrophages retained high plasticity and functional diversity. The balance between the M1 and M2 subsets is the hub of pro-inflammatory and anti-inflammatory reactions, which mediate immune homeostasis during tissue regeneration and repair.[18] Therefore, the divergent expression of anti- and pro-inflammatory factors in the two groups observed in vitro underlies the chirality-dependent tissue homeostasis in vivo. These results indicated that macrophages recognized the difference of chiral nanostructures and polarized to divergent phenotypes. Our finding was consistent with the previous finding on the effect of molecular chirality on immunity that ʟ-chiral interface promote M2-type polarization of macrophages and showed the effect of M-chirality is stronger than that of P-chirality.[19]

To analyze the difference in the downstream immune response caused by chirality-dependent macrophage polarization, microarray analysis was performed. Cluster analysis showed that overexpressed genes of macrophages in the M group were mainly related to the biological process of immune response (Figure 3d). The results of gene ontology analysis and pathway enrichment analysis also showed that complement receptor-mediated signaling pathway, G-protein-coupled receptor signaling pathway, toll-like receptor signaling pathway, and phospholipase C-activating G-protein-coupled receptor signaling pathway were activated (Figure 3e–g). Complement receptor-mediated signaling pathway mediates immune homeostasis by regulating complement activation. Chemokines secreted by immune cells play a role via G protein. Moreover, toll-like receptor signaling pathway and phospholipase C-activating G-protein-coupled receptor signaling pathway activate immune cells and regulate their functions.[20] The activation of the above biological pathways in the M group would help to manipulate immunological response for restoring homeostasis. These results indicated that the macrophages in the M group had a stronger immune activation and regeneration effect than those in the P group. The volcano plot showed that the expression of *CD206* and *ARG1* in the M group was upregulated compared with the P group (Figure 3e), further confirming the results of the phenotype experiment. Gene enrichment analysis revealed that autophagy and sphingolipid metabolism-related genes related to M2 polarization were enriched in the M group (Figure 3h). Autophagy regulates macrophage polarization, inhibiting M1-type differentiation and promoting M2-type differentiation. Loss of autophagy may lead to increased inflammation by inhibiting the differentiation of macrophages into the M2 phenotype.[21] Sphingosine-1-phosphate in sphingolipid metabolism also promotes M2 polarization of macrophages.[22] Therefore, the results of the in vitro experiments indicate that the higher capability of M-nanofibrils in restoring homeostasis is attributed to the upregulated M2 macrophage polarization and the series of downstream immunological signaling pathways.

Next, we investigated the mechanism underlying the chirality-dependent macrophage polarization. On the basis of the in-depth pathways analysis of microarray data, we performed immunofluorescence staining, RT-qPCR and western blotting. All these assays showed that the expression of Itgβ1, pFAK, and vinculin was significantly upregulated in the M group (**Figure** 4a–c). The higher expression of Itgβ1 and vinculin indicated that more cell-chiral structure focal adhesions had formed in the M group than in the P group. Moreover, the higher expression of pFAK in the cellular adhesion complex indicates the longer lifespan of focal adhesions in the M group than in the P group.[23] These results suggested that mechanosensing was activated in the M group more than in the P group. Furthermore, mechanically coupled with integrins by vinculin, the organization of the cytoskeleton and myosin was also found to be regulated by chirality (Figure 4a–c). 3D morphology reconstruction indicated that macrophages in the M group had more protrusions than those in the P group (Figure 4f), which is consistent with the morphology of different macrophage types. Unlike the in-plane spreading of cells cultured on 2D substrate, 3D matrix facilitate cellular protruding in various direction and yield spherical cellular morphology.[24] Additionally, quantitative analysis revealed that the cell volume and cell stiffness were significantly higher and cell sphericity was significantly lower in the M group than in the P group (Figure 4g–i), indicating the higher cellular contractile stress in the M group than in the P group. The upregulation of mechanosensing and cellular contractile stress in the M group was corroborated by the gene clustering results in microarray analysis (Figure 4d). Moreover, RT-qPCR, western blotting, and cytometry demonstrated that the cellular contractile stress and M2-type polarization in the M group could be greatly reduced through FAK inhibition (Figure 4e,j and Figure S5, Supporting Information). These findings demonstrate that different macrophage polarization may be initiated by chirality-dependent mechanosensing and downstream cellular contractile stress (Figure 4k).

We further investigated how the above cell-chiral structure interaction was translated into intracellular molecular signals for guiding macrophage polarization. Our previous study showed that chirality determined stem cell fate by regulating the nuclear transfer of YAP,[25] however, macrophages cultured in a chiral environment showed no significant difference in YAP expression and location (Figure S6, Supporting Information). YAP also plays an important role in M1 polarization of macrophages.[24b] In this work, the expression of M1 markers showed no significant difference. On the other hand, a critically important mechanosensor of the ion channel PIEZO1 was found to be upregulated in the M-group compared with the P group through immunofluorescence staining and flow cytometry (**Figure** 5a). Downstream, the intracellular Ca^{2+} concentration and nuclear translocation and phosphorylation of STAT were found to be significantly higher in the M group than in the P group (Figure 5c and Figure S7, Supporting Information). It has been reported that the influx of Ca^{2+} mediates the signals of PIEZO1 to STAT, whereas the nuclear translocation and phosphorylation of STAT favors M2 polarization of macrophages to inhibit inflammation.[26] Furthermore, RT-qPCR and western blotting demonstrated that signals of CXCL2, COL2A1, and COL9A2 downstream of PIEZO1 were significantly upregulated in the M group compared with the P group (Figure 5e). Of these, CXCL2—a classic chemokine—was activated by Ca^{2+} to promote stem cell chemotaxis (Figure 5g).
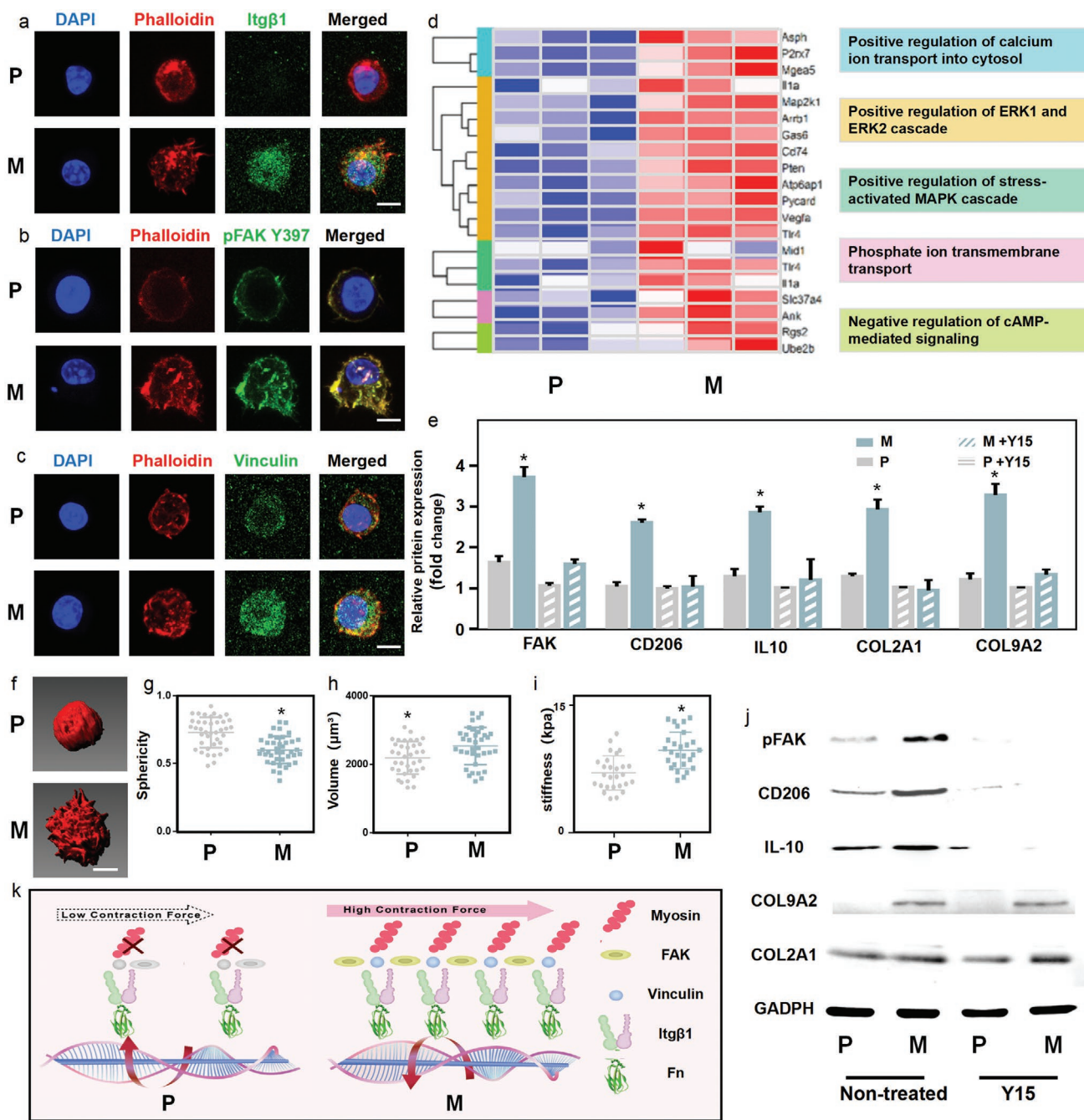
Figure 4. M-nanofibrils induced higher mechanosensation and cellular contractile stress than P-nanofibrils. Immunofluorescence staining shows that a) Itgβ1, b) pFAK, and c) vinculin were significantly upregulated in the M group. d) Hierarchical gene clustering shows upregulated mechanosensing and mechanotransduction genes in the M group. e) RT-qPCR shows upregulated levels of mechanosensing and mechanotransduction genes (*FAK, CD206, IL10, COL2A1, COL9A2*). f) Representative microscopy images of macrophages cultured in matrixes for 24 h, visualized by F-actin-positive pixel reconstruction and the g) volume and h) sphericity analyzed using Imaris (phalloidin, reconstruction [RC]). Scale bars: 5 μm. i) Quantification of MSC stiffness showing that the cells on M chirality matrix were stiffer than the cells on P chirality matrix, as measured by AFM. j) Western blot showing upregulated levels of mechanosensing and mechanotransduction proteins (pFAK, STAT, COL2A1) in M group. k) A schematic representation of chirality-dependent mechanosensation and cellular contractile stress. Data are the means ± SEM. *$P < 0.05$, one-way ANOVA (e,g,h,i).

COL2A1 and COL9A2 were upregulated by pSTAT6 to promote osteogenic differentiation of mesenchymal stem cells (Figure 5g).[27] As such, the differential expression of these signals laid the foundation for chirality-dependent tissue regeneration. Moreover, the upregulation of these molecular signals, the increased M2 polarization of macrophages, and stem cell migration and differentiation in the ʟ group were found to be significantly reduced by PIEZO1 inhibition (Figure 5e,g,h and Figures S8 and S9, Supporting Information). Therefore, the greater activation of the ion channel PIEZO1 in M-nanofibrils
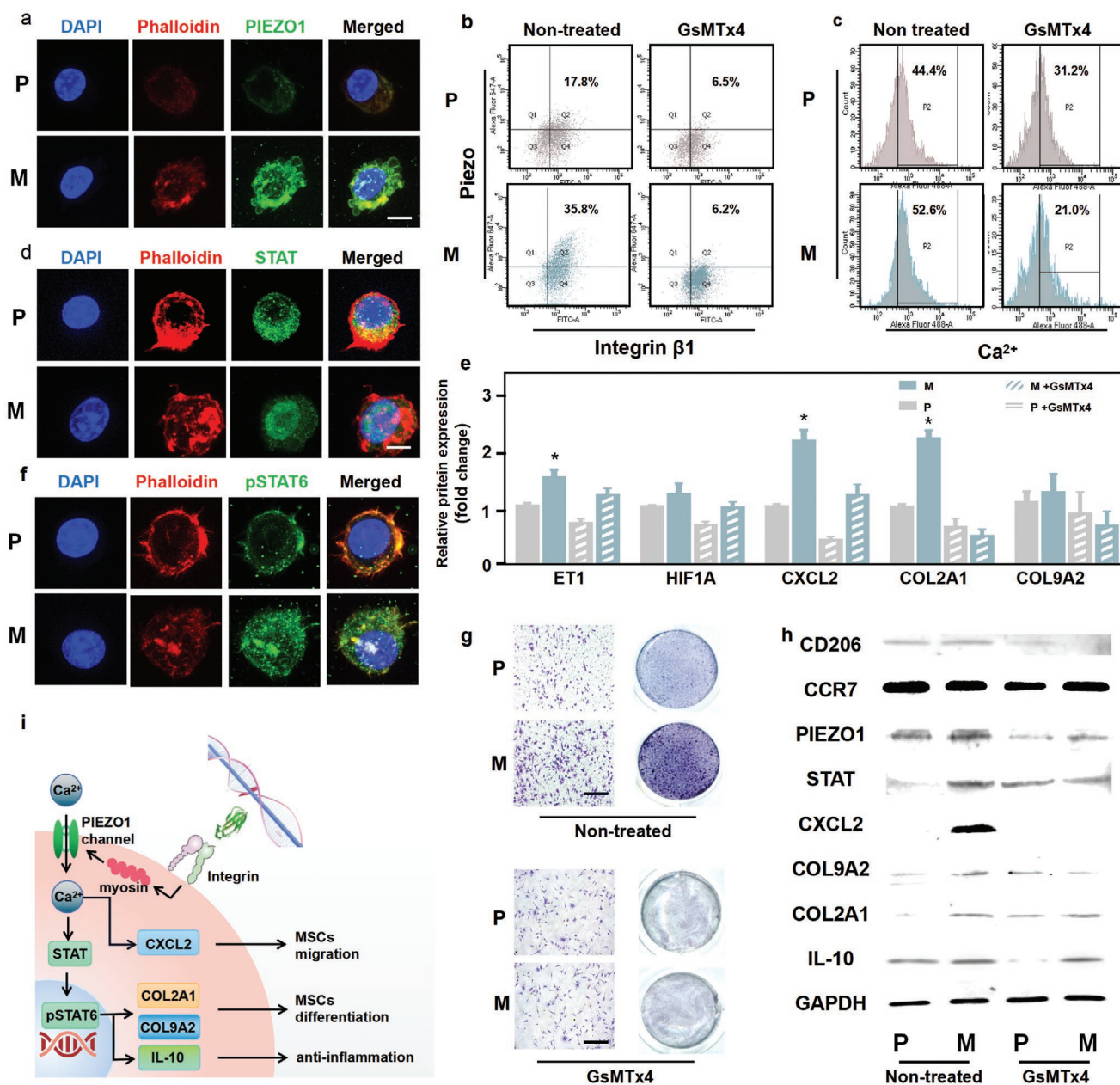
Figure 5. Ion channel PIEZO1 transduced chirality-dependent cellular contractile stress to intracellular cascades for guiding tissue homeostasis. a) Immunofluorescence staining and b,c) flow cytometry show that PIEZO1 was upregulated in the M group, which enhanced the Ca^{2+} influx. Immunofluorescence staining shows that d) nuclear translocation and f) phosphorylation of STAT were significantly higher in the M group than in the P group. e) RT-qPCR shows that the inhibition of PIEZO1 significantly decreased the expression of *COL2A1*, *COL9A2*, and PIEZO1 downstream genes (*ET1*, *HIF1A*, *CXCL2*). g) Transwell culture and ALP staining show that stem cell migration and differentiation in the M group were significantly reduced after PIEZO1 inhibition. h) Western blotting analysis revealing the upregulation of PIEZO1, STAT, CXCL2 in the M group. i) A schematic representation of the molecular signaling pathway through which PIEZO1 transduces chirality-dependent cellular contractile stress to intracellular cascades for guiding tissue homeostasis. Data are the means ± SEM. *$P < 0.05$, one-way ANOVA (e).

than in P-nanofibrils may enhance the nuclear transfer of STAT and downstream CXCL2, COL2A1, and COL9A2 to facilitate the M2 polarization of macrophages for inflammation inhibition and promote stem cell chemotaxis and differentiation for tissue regeneration (Figure 5i). It has been reported that PIEZO1 is activated by myosin movement along the cytoskeleton.[28] In this study, we have revealed that chirality of nanofibrils significantly

influenced cellular contractile stress by inducing different organization of the cytoskeleton and myosin. Moreover, our results also showed that cellular contractile stress is decreased by inhibition of pFAK, resulting in the downregulation of PIEZO1 and downstream effector expression. Taken together, molecular analysis demonstrated that the ion channel PIEZO1, rather than the classical mechano-rheostat YAP, played a critical
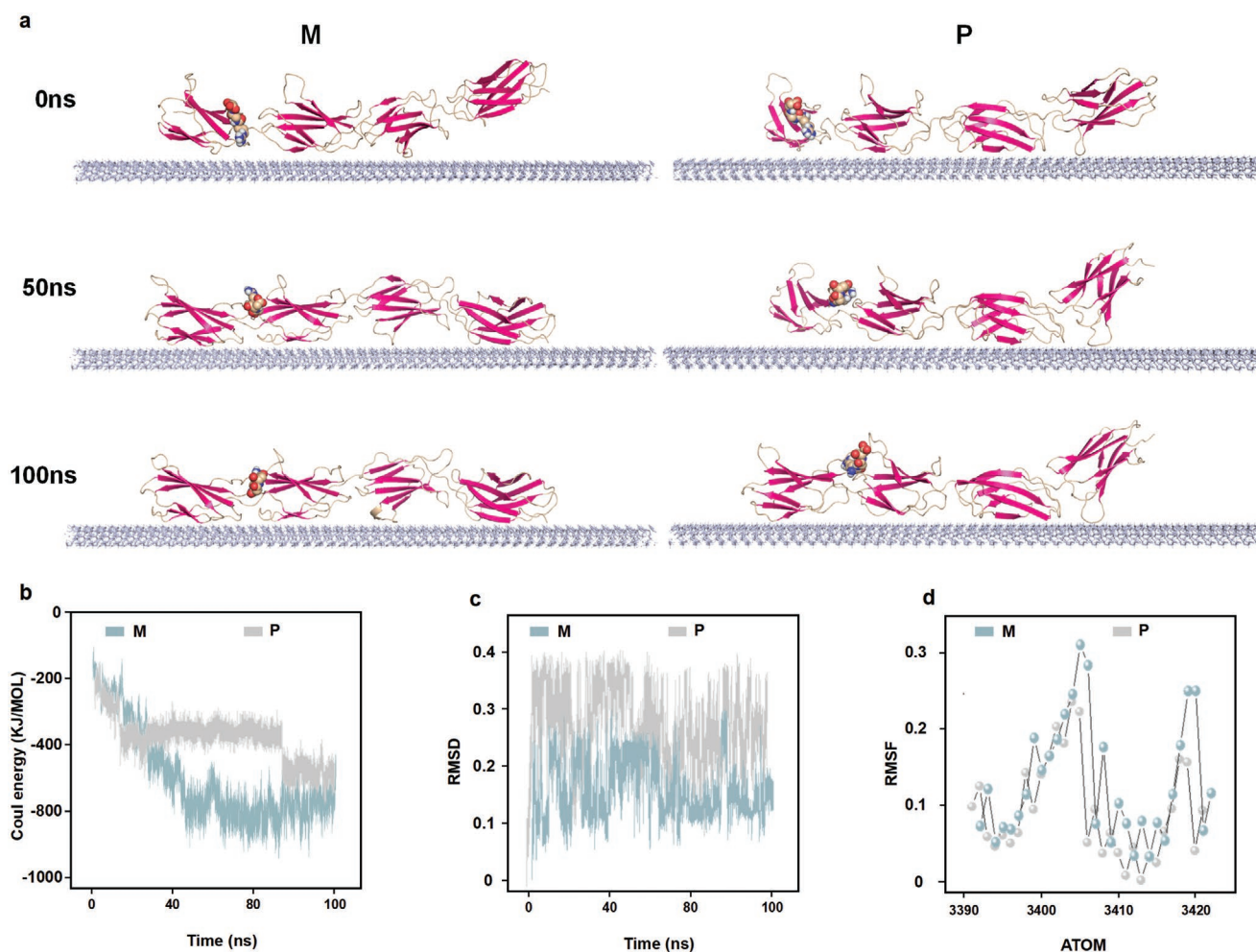
Figure 6. M-nanofibrils showed a higher stereo-affinity to the binding agent than P-nanofibrils in classical molecular dynamic simulations. a) Snapshots showing the effect of chirality on FnIII7-10 tethering. b) Computed average interaction energies showing the lower Coulomb energy that is required during recognition between M-nanofibrils and FnIII7-10 than that between P-nanofibrils and FnIII7-10. The root-mean-square deviation (RMSD; c) root-mean-square fluctuation (RMSF); d) values of the RGD residues showing higher interdomain elasticity and flexibility of the RGD configuration in the M-nanofibril-FnIII7-10 complex than in the P-nanofibril-FnIII7-10 complex.

role during transduction of chiral stimuli in macrophages and was mechanically activated by chirality-dependent cellular contractile stress.

We also explored how cells recognize the physiological and pathological chirality to induce divergent downstream cellular processes. It is well established that FnIII7-10, as the key cell-binding domains of fibronectin (FN), plays a vital role in mediating cell–material interaction.[29] Therefore, we performed a classical molecular dynamics simulation to explore the recognition between FnIII7-10 and chiral nanofibers. The snapshot showed that FnIII7-10 accomplished the recognition and binding with the M-nanofibrils within 50 ns. However, FNIII7-10 did not form a stable association with the P-nanofibrils until 100 ns (**Figure 6**a, S10). This result indicated that M-nanofibrils showed a higher stereo-affinity to FnIII7-10 than P-nanofibrils. This phenomenon was corroborated by the lower LJ interaction energy (-800 kJ mol^{-1} for M-nanofibrils vs -600 kJ mol^{-1} for P-nanofibrils) and Coulomb interaction energy (-900 kJ mol^{-1} for M-nanofibrils-FnIII7-10 complex vs -700 kJ mol^{-1} for P-nanofibrils-FnIII7-10 complex; Figure 6b

and Figure S11, Supporting Information). Furthermore, a markedly different configuration of RGD residue in FnIII7-10 was found in response to chirality. The root-mean-square deviation (0.15 for M-nanofibrils vs 0.25 for P-nanofibrils; Figure 5c) and root-mean-square fluctuation (0.17 nm for M-nanofibrils vs 0.13 nm for P-nanofibrils; Figure 5d) values for RGD indicated a higher interdomain elasticity and flexibility of RGD in the M-nanofiber-FnIII7-10 complex than in the P-nanofiber-FnIII7-10 complex, which may facilitate integrin binding.[30] These data demonstrated that chiral nanofibrils affect the stereo-affinity and conformation of the binding ligand to induce divergent cell adhesion, paving the way for guiding chirality-dependent cellular contractile stress.

3. Conclusion

In this study, we studied the in vivo and in vitro immunological response and the spatiotemporal cascades of macrophages in response to 3D chiral supramolecular structures. We showed

that pathology-mimetic M-nanofibrils—but not physiology-mimetic P-nanofibrils—act as a defense mechanism that upregulates M2 macrophage polarization and activates downstream immune signaling to restore tissue homeostasis. More importantly, we discovered the critical role of the ion channel PIEZO1 rather than the classical mechano-rheostat YAP in the outside-in transduction of chirality in macrophages. Additionally, theoretical simulation demonstrated the interfacial enantioselective mechanism of chirality recognition: M-nanofibrils showed higher multi-stereo compatibility to the cell-binding agent than P-nanofibrils. These findings underscore the structural mechanisms of aging and disease. The revealed key molecular signals mediating chirality-dependent immunological response will shed light on the dynamics of tissue homeostasis occurring under physiological and pathological conditions. Our findings will also provide a more practical, simple, and efficient material strategy for regulating macrophages to treat disease.

Supporting Information

Supporting Information is available from the Wiley Online Library or from the author.

Conflict of Interest

The authors declare no conflict of interest.

Data Availability Statement

Research data are not shared.

[1] J. Nikolich-Žugich, *Nat. Immunol.* **2018**, *19*, 10.
[2] a) P. G. Wolynes, *Proc. Natl. Acad. Sci. USA* **1996**, *93*, 14249; b) X. Yao, X. Wang, J. Ding, *Acta Biomater.* **2021**, *126*, 92.
[3] a) P. M. Helfman, J. L. Bada, *Nature* **1976**, *262*, 279; b) V. A. Tverdislov, E. V. Malyshko, *Symmetry* **2020**, *12*, 587; c) G.-F. Chen, T.-H. Xu, Y. Yan, Y.-R. Zhou, Y. Jiang, K. Melcher,

H.-E. Xu, *Acta Pharmacol. Sin.* **2017**, *38*, 1205; d) K. Ariga, *Small Sci.* **2021**, *1*, 2000032.
[4] N. Fujii, T. Takata, N. Fujii, K. Aki, H. Sakaue, *Biochim. Biophys. Acta, Proteins Proteomics* **2018**, 1866.840.
[5] a) S. Ohtani, *Int. J. Legal Med.* **2002**, *116*, 361; b) S. Ohtani, T. Yamamoto, *J. Forensic Sci.* **2005**, *50*, 1020; c) T. Monum, C. Jaikang, A. Sinthubua, S. Prasitwattanaseree, P. Mahakkanukrauh, *Aust. J. Forensic Sci.* **2017**, *51*, 417.
[6] a) D. R. Griffin, M. M. Archang, C.-H. Kuan, W. M. Weaver, J. S. Weinstein, A.-C. Feng, A. Ruccia, E. Sideris, V. Ragkousis, J. Koh, M. V. Plikus, D. D. Carlo, T. Segura, P. O. Scumpia, *Nat. Mater.* **2021**, *20*, 560; b) M. Suzuki, T. Sujino, S. Chiba, Y. Harada, M. Goto, R. Takahashi, M. Mita, K. Hamase, T. Kanai, M. Ito, M. K. Waldor, M. Yasui, J. Sasabe, *Sci. Adv.* **2021**, *7*, eabd6480.
[7] a) E. Danelius, R. G. Ohm, A. Ahsanullah, M. Mulumba, H. Ong, S. Chemtob, M. Erdélyi, W. D. Lubell, *J. Med. Chem.* **2019**, *62*, 11071; b) T. Sun, D. Han, K. Rhemann, L. Chi, H. Fuchs, *J. Am. Chem. Soc.* **2007**, *129*, 1496; c) S. Khan, J. J. Weterings, C. M. Britten, A. R. Jong, D. Graafland, C. J. M. Melief, S. H. Burg, G. Marel, H. S. Overkleeft, D. V. Filippov, F. Ossendorp, *Mol. Immunol.* **2009**, *46*, 1084.
[8] a) M. Zielińska-Przyjemska, F. K. Główka, J. Klaczyńska, *Chirality* **2008**, *20*, 159; b) Y. Wang, Z. Jiang, W. Xu, Y. Yang, X. Zhuang, J. Ding, X. Chen, *ACS Appl. Mater. Interfaces* **2019**, *11*, 8725; c) F. Neubrech, M. Hentschel, N. Liu, *Adv. Mater.* **2020**, *32*, 1905640.
[9] L. Zhang, L. Qin, X. Wang, H. Cao, M. Liu, *Adv. Mater.* **2014**, *26*, 6959.
[10] a) K Beck, B Brodsky, *J. Struct. Biol.* **1998**, *122*, 17; b) U. Eliav, G. Navon, *J. Am. Chem. Soc.* **2006**, *128*, 15956.
[11] a) N. Rubin, E. Perugia, M. Goldschmidt, M. Fridkin, L. Addadi, *J. Am. Chem. Soc.* **2008**, *130*, 4602; b) V. Soontornniyomki, C. Choi, J. Pomakian, H. V. Vinters, *Hum. Pathol.* **2010**, *41*, 1601; c) A. Biffi, S. M. Greenberg, *J. Clin. Neurol.* **2011**, *7*, 6915; d) N. Gao, Z. Du, Y. Guan, K. Dong, J. Ren, X. Qu, *J. Am. Chem. Soc.* **2019**, *141*, 6915.
[12] K. Okamoto, T. Nakashima, M. Shinohara, T. Negishi-Koga, N. Komatsu, A. Terashima, S. Sawa, T. Nitta, H. Takayanagi, *Physiol. Rev.* **2017**, *97*, 1295.
[13] D. F. Fiorentino, A. Zlotnik, T. R. Mosmann, M. Howard, A. O'Garra, *J. Immunol.* **1991**, *147*, 3815.
[14] S. R. Voss, D. Murrugarrab, T. B. Jensenc, J. R. Monaghan, *Comp. Biochem. Physiol., Part C: Toxicol. Pharmacol.* **2018**, *208*, 53.
[15] a) D. K. V. Kumar, S. H. Choi, K. J. Washicosky, W. A. Eimer, S. Tucker, J. Ghofrani, A. Lefkowitz, G. McColl, L. E. Goldstein, R. E. Tanzi, R. D. Moir, *Sci. Transl. Med.* **2016**, *8*, 340ra72; b) W. A. Eimer, D. K. V. Kumar, N. K. N. Shanmugam, A. S. Rodriguez, T. Mitchell, K. J. Washicosky, B. György, X. O. Breakefield, R. E. Tanzi, R. D. Moir, *Neuron* **2018**, *99*, 56; c) J. Kumara, H. Erañab, E. Lopez-Martíneza, N. Claesc, V. F. Martínd, D. M. Solíse, S. Balsc, A. L. Cortajarenaa, J. Castillab, L. M. Liz-Marzán, *Proc. Natl. Acad. Sci. USA* **2018**, *115*, 3225; d) Y. Li, C. Zhao, F. Luo, Z. Liu, X. Gu, Z. Luo, X. Zhang, D. Li, C. Liu, X. Li, *Cell Res.* **2018**, *28*, 897; e) A. Faridi, Y. Sun, Y. Okazaki, G. Peng, J. Gao, A. Kakinen, P. Faridi, M. Zhao, I. Javed, A. W. Purcell, T. P. Davis, S. Lin, R. Oda, F. Ding, P. C. Ke, *Small* **2018**, *14*, 1802825; f) J.-Y. Hur, G. R. Frost, X. Wu, C. Crump, S. J. Pan, E. Wong, M. Barros, T. Li, P. Nie, Y. Zhai, J. C. Wang, J. Tcw, L. Guo, A. McKenzie, C. Ming, X. Zhou, M. Wang, Y. Sagi, A. E. Renton, B. T. Esposito, Y. Kim, K. R. Sadleir, I. Trinh, R. A. Rissman, R. Vassar, B. Zhang, D. S. Johnson, E. Masliah, P. Greengard, A. Goate, Y.-M. Li, *Science* **2020**, *586*, 735; g) P. H. Nguyen, A. Ramamoorthy, B. R. Sahoo, J. Zheng, P. Faller, J. E. Straub, L. Dominguez, J.-E. Shea, N. V. Dokholyan, A. De Simone, B. Ma, R. Nussinov, S. Najafi, S. T. Ngo, A. Loquet, M. Chiricotto, P. Ganguly, J. McCarty, M. S. Li, C. Hall, Y. Wang, Y. Miller, S. Melchionna, B. Habenstein, S. Timr, J. Chen, B. Hnath, B. Strodel, R. Kayed, S. Lesné, G. Wei, F. Sterpone, A. J. Doig, P. Derreumaux, *Chem. Rev.* **2021**, *121*, 2545.

**ADVANCED
SCIENCE NEWS**

www.advancedsciencenews.com

**ADVANCED
MATERIALS**

www.advmat.de

[16] J. Li, X. Jiang, H. Li, M. Gelinsky, Z. Gu, *Adv. Mater.* **2021**, *33*, 2004172.

[17] a) B.-H. Cha, S. R. Shin, J. Leijten, Y.-C. Li, S. Singh, J. C. Liu, N. Annabi, R. Abdi, M. R. Dokmeci, N. E. Vrana, A. M. Ghaemmaghami, A. Khademhosseini, *Adv. Healthcare Mater.* **2017**, *6*, 1700289; b) Q. Yao, J. Liu, Z. Zhang, F. Li, C. Zhang, B. Lai, L. Xiao, N. Wang, *J. Biol. Chem.* **2018**, *293*, 16572.

[18] a) S. J. Forbes, N. Rosenthal, *Nat. Med.* **2014**, *20*, 857; b) G. Yun, S.-Y. Tang, H. Lu, S. Zhang, M. D. Dickey, W. Li, *Small Sci.* **2021**, *1*, 2000080.

[19] Y. Duan, H. Zheng, Z. Li, Y. Yao, J. Ding, X. Wang, J. R. Nakkal, D. Zhang, Z. Wang, X. Zuo, X. Zheng, J. Ling, C. Gao, *Biomaterials.* **2020**, *246*, 120012.

[20] a) X. Zhang, Y. Kimura, C. Fang, L. Zhou, G. Sfyroera, J. D. Lambris, R. A. Wetsel, T. Miwa, W.-C. Song, *Blood* **2007**, *110*, 228; b) W. Spivia, P. S. Magno, P. Le, D. A. Fraser, *Inflammation Res.* **2014**, *63*, 885; c) S.-J. Zhao, H. Liu, J. Chen, D.-F. Qian, F.-Q. Kong, J. Jie, G.-Y. Yin, Q.-Q. Li, J. Fan, *J. Bone Miner. Res.* **2015**, *35*, 2015; d) M. Zhu, S. Wang, *Small Sci.* **2021**, *1*, 2000056.

[21] K. Liu, E. Zhao, G. Ilyas, G. Lalazar, Y. Lin, M. Haseeb, K. E. Tanaka, M. J. Czaja, *Autophagy* **2015**, *11*, 271.

[22] A. Weigert, N. Tzieply, A. Knethen, A. M. Johann, H. Schmidt, G. Geisslinger, B. Brune, *Mol. Biol. Cell.* **2007**, *18*, 3810.

[23] B. Cheng, W. Wan, G. Huang, Y. Li, G. M. Genin, M. R. K. Mofrad, T. J. Lu, F. Xu, M. Lin, *Sci. Adv.* **2020**, *6*, eaax1909.

[24] Y. Su, M. S. Toftdal, A. L. Friec, M. Dong, X. Han, M. Chen, *Small Sci.* **2021**, *1*, 2100003.

[25] a) Y. Wei, S. Jiang, M. Si, X. Zhang, J. Liu, Z. Wang, C. Cao, J. Huang, H. Huang, L. Chen, S. Wang, C. Feng, X. Deng, L. Jiang, *Adv. Mater.* **2019**, *31*, 1900582; b) X. Zhou, W. Li, S. Wang, P. Zhang, Q. Wang, J. Xiao, C. Zhang, X. Zheng, X. Xu, S. Xue, L. Hui, H. Ji, B. Wei, H. Wang, *Cell Rep.* **2019**, *27*, 1176.

[26] a) N. Wang, H. Liang, K. Zeng, *Front. Immunol.* **2014**, *5*, 614; b) S. C.-C. Huang, A. M. Smith, B. Everts, M. Colonna, E. L. Pearce, J. D. Schilling, E. J. Pearce, *Immunity* **2016**, *45*, 817; c) C. Chen, A. D. Smith, L. Cheung, Q. Pham, J. F. Urban Jr., H. D. Dawson, *Front. Immunol.* **2020**, *11*, 605.

[27] a) B. J. O'Brien, H. A. Singer, A. P. Aadam, R. G. Ginnan, *FASEB J.* **2021**, *35*, e21437; b) W. Mei, D. Song, Z. Wu, L. Yang, P. Wang, R. Zhang, X. Zhu, *Ecotoxicol. Environ. Saf.* **2021**, *214*, 112080.

[28] a) J. L. Nourse, M. M. Pathak, *Semin. Cell. Dev. Biol.* **2017**, *11*, 3; b) M. B. Hilscher, T. Sehrawat, J. P. Arab, Z. Zeng, J. Gao, M. Liu, E. Kostallari, Y. Gao, D. A. Simonetto, U. Yaqoob, S. Cao, A. Revzin, A. Beyder, R. A. Wang, P. S. Kamath, P. Kubes, V. H. Shah, *Gastroenterology* **2019**, *157*, 193; c) W.-C. Hung, J. R. Yang, C. L. Yankaskas, B. S. Wong, P.-H. Wu, C. Pardo-Pastor, S. A. Serra, M.-J. Chiang, Z. Gu, D. Wirtz, M. A. Valverde, J. T. Yang, J. Zhang, K. Konstantopoulos, *Cell Rep.* **2016**, *15*, 1430; d) A. G. Solis, P. Bielecki, H. R. Steach, L. Sharma, C. C. D. Harman, S. Yun, M. R. de Zoete, J. N. Warnock, S. D. Filip To, A. G. York, M. Mack, M. A. Schwartz, C. S. Dela Cruz, N. W. Palm, R. Jackson, R. A. Flavell, *Nature* **2019**, *573*, 69.

[29] a) C. Fischbach, G. G. Malliaras, A. M. D. Wan, R. M. Schur, D. Gourdon, C. K. Ober, *Adv. Mater.* **2012**, *24*, 2501; b) N. E. Muzzio, M. A. Pasquale, X. Rios, O. Azzaroni, J. Llop, S. E. Moya, *Adv. Mater. Interfaces* **2019**, *6*, 1900008; c) Z. Chen, F. Hu, Z. Lin, J. Hu, R. Shen, Y. Lin, X. Y. Liu, *Small Sci.* **2021**, *1*, 2000049.

[30] K. H. Vining, D. J. Mooney, *Nat. Rev. Mol. Cell Biol.* **2017**, *18*, 728.